Computers in Biology and Medicine 41 (2011) 1166–1177

Contents lists available at ScienceDirect

Computers in Biology and Medicine

journal homepage: www.elsevier.com/locate/cbm

Extracting biomarkers of autism from MEG resting-state functional connectivity networks

Vassilis Tsiaras [a,*], Panagiotis G. Simos [b], Roozbeh Rezaie [c], Bhavin R. Sheth [d], Eleftherios Garyfallidis [e], Eduardo M. Castillo [c], Andrew C. Papanicolaou [c]

[a] Computer Science Department, University of Crete, Heraklion, Crete, GR-71409, Greece
[b] Department of Psychology, University of Crete, Rethymno, Crete, GR-74100, Greece
[c] Department of Pediatrics, University of Texas Health Science Center-Houston, United States
[d] Department of Electrical & Computer Engineering, University of Houston 77204, United States
[e] MRC Cognition and Brain Sciences Unit, Cambridge CB27EF, UK

ARTICLE INFO

Keywords:
Autism spectrum disorders
MEG
Resting-state functional connectivity
Interdependence measures
Network analysis
Graph theory

ABSTRACT

The present study is a preliminary attempt to use graph theory for deriving distinct features of resting-state functional networks in young adults with autism spectrum disorder (ASD). Networks modeled neuromagnetic signal interactions between sensors using three alternative interdependence measures: (a) a non-linear measure of generalized synchronization (robust interdependence measure [RIM]), (b) mutual information (MI), and (c) partial directed coherence (PDC). To summarize the information contained in each network model we employed well-established global graph measures (average strength, assortativity, clustering, and efficiency) as well as graph measures (average strength of edges) tailored to specific hypotheses concerning the spatial distribution of abnormalities in connectivity among individuals with ASD. Graph measures then served as features in leave-one-out classification analyses contrasting control and ASD participants. We found that combinations of regionally constrained graph measures, derived from RIM, performed best, discriminating between the two groups with 93.75% accuracy. Network visualization revealed that ASD participants displayed significantly reduced interdependence strength, both within bilateral frontal and temporal sensors, as well as between temporal sensors and the remaining recording sites, in agreement with previous studies of functional connectivity in this disorder.

1. Introduction

Autism spectrum disorders (ASD) are a family of pervasive developmental disorders believed to reflect abnormalities in brain development. ASD is characterized by deficits in communication, social interaction, and a limited range of interests with repetitive stereotypical behavior [1–4]. The exact cause of autism is unknown, though many studies have noted differences in structure and function of the brains of individuals with autism. Several reports have commented on potential abnormalities in total brain volume [5,6] and regional changes in gray matter volume and/or cortical thickness [7–10]. Changes in white matter integrity [11–13] may also reflect abnormal connectivity between specific brain regions, resulting in deficient integration of information at the neural level [2,14,15]. These findings are consistent with reports of abnormal cortical connectivity in ASD during execution of tasks posing high cognitive demands. Most studies report weaker connectivity [16,15,17–19], while others report stronger connectivity [20,21]. Interestingly, hemodynamic imaging studies have also highlighted alterations in diffuse patterns of regional connectivity in ASD during rest [22–24]. Electromagnetic recordings lend further support to this claim. For example, using dense array EEG, Murias et al. [25] reported differences between adults with ASD and healthy, age-matched controls, consisting of increased theta-band coherence between temporal and frontal regions, and reduced alpha coherence between anterior and posterior regions, in the former group of individuals. Moreover, Coben et al. [26] reported reduced intra-hemispheric delta and theta coherences for both short to medium and longer inter-electrode distances, as well as reduced inter-hemispheric delta and theta coherences in the frontal and temporal regions, relative to controls. Additionally, abnormalities in baseline activity in ASD were highlighted using magnetoencephalography (MEG), though these have consisted of patterns of visually distinct epileptiform activity [27,28], similar to those seen in children with Landau–Kleffner syndrome.

* Corresponding author.
E-mail addresses: tsiaras@csd.uoc.gr (V. Tsiaras), psimos@psy.soc.uoc.gr (P.G. Simos), Roozbeh.Rezaie@uth.tmc.edu (R. Rezaie), brsheth@uh.edu (B.R. Sheth), eleftherios.garyfallidis@mrc-cbu.cam.ac.uk (E. Garyfallidis), eduardo.m.castillo@uth.tmc.edu (E.M. Castillo), Andrew.C.Papanicolaou@uth.tmc.edu (A.C. Papanicolaou).

0010-4825/$ - see front matter © 2011 Elsevier Ltd. All rights reserved.
doi:10.1016/j.compbiomed.2011.04.004

If aberrant network organization is a constitutional characteristic of ASD, then it may be evident in spatiotemporal profiles of baseline neurophysiological activity. The present study is a preliminary attempt to use graph theory for deriving potentially distinct features of MEG based resting-state functional networks in young adults with autism. Graph measures have been applied to topological analysis of brain functional networks, and many of them have been shown to reflect disease and statistically significant differences between healthy subjects and subjects with neurological or psychiatric disorders such as ASD [29]. Graph theory offers a unique perspective and a common framework for studying interactions between neighboring and remote cortical areas, with areas corresponding to the vertices and interactions to the edges of a graph-based network [30].

Network vertices can easily be identified with fMRI data but the dependence between vertices can be measured only for low frequencies (<0.5 Hz) due to the limited time resolution of fMRI. On the other hand the time resolution of EEG/MEG is excellent but the mapping from generators in the brain to the sensors on the scalp is complex and the topology of a network in sensor space differs from the topology in generators space [31]. To identify generators from EEG/MEG data one has to solve the inverse problem which is ill posed and sensitive to noise. In this work, where our objective was to distinguish ASD from typically developing participants using MEG, we explored information present in sensor-level functional networks avoiding the ambiguities which are introduced by the solution of the inverse problem. In sensor-level functional networks vertices correspond to sensors. We estimated the interactions between vertices from neuromagnetic recordings of resting-state brain activity by applying two alternative bivariate and one multivariate interdependence measures: (a) a non-linear measure of generalized synchronization (robust interdependence measure (RIM)), (b) mutual information (MI), and (c) partial directed coherence (PDC). MI is based on solid information-theory concepts. RIM is a heuristic, which is based on the theory of recurrence within dynamic systems. Traditional coherence estimates were also computed for comparison [32]. All these measures are bivariate and suffer from the problem of detecting spurious synchronization between conditionally independent variables. For example, if X drives Y and Z but there is no direct connection between X and Y then, erroneously, any bivariate measure will detect high dependence between Y and Z. This problem is, in principle, addressed by using multivariate measures such as PDC.

The information contained in a synchronization network can be further summarized with graph measures. Here we considered well-established graph measures originally derived from statistical physics, such as the average strength, the clustering coefficient, the assortativity coefficient and the global efficiency index, as well as graph measures tailored to specific hypotheses concerning the spatial distribution of abnormalities in connectivity among individuals with ASD. These custom connectivity indices were derived by segmenting the sensor array into sectors and estimating connectivity both within- and between-sectors, presumed to reflect ongoing neurophysiological activity in frontal, temporal, parietal, ventral occipitotemporal and occipital brain regions. Then we investigated the capacity of these graph measures to distinguish individuals from the two groups. Our main finding was that graph measures that incorporate previous knowledge on differences in connectivity among ASD and control subjects outperform commonly used, but global, graph measures as classification features. Additionally we discuss how the classification results are affected by signal spectral frequency and by the interdependence metric used to obtain the network models. Finally we illustrate the differences between ASD and control subjects by visualizing the average spatial network profile for each group as well as representing the spatial distribution of edges that are stronger in the absolute majority of ASD participants compared to the majority of control participants.

2. Methodology

Initially, functional connectivity networks were constructed in sensor space using synchronization measures. Then potentially characteristic features of a mental disorder, in the present case autism, were extracted from these networks using graph measures. The ability of a feature in differentiating between two or more groups of subjects was evaluated by performing cross-validation classification tests and/or ANOVAs. This method is illustrated step-by-step in Fig. 1. In the following we assume that we have two

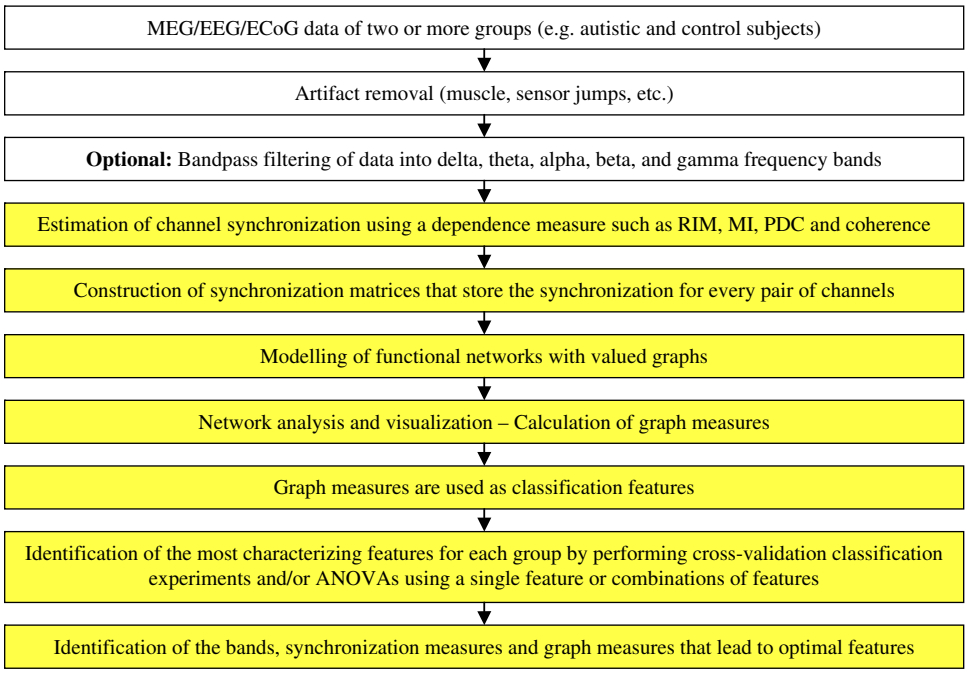

Fig. 1. Outline of the proposed methodology. In this paper we focus on steps represented by rectangles highlighted in yellow (steps 4–10). (For interpretation of the references to color in this figure legend, the reader is referred to the web version of this article.)

groups of subjects (ASD and controls). Also without loss of generality we assume that for each subject a continuous multivariate (MEG) signal of duration 150 s and sampling frequency 1017 Hz is available.

2.1. Synchronization measures

For each subject, synchronization matrices were computed using both bivariate and multivariate synchronization measures. The bivariate measures were (a) a non-linear measure of generalized synchronization (robust interdependence measure (RIM)) and (b) mutual information (MI), while partial directed coherence (PDC) served as the multivariate measure. The entire 150 s trace was used as input for computing MI and PDC. Computation of RIM was performed on 25 consecutive 6 s segments; a synchronization matrix was computed for each 6-s segment and finally the average (across all the 6-s segments) synchronization matrix was calculated. The sensitivity of each measure was initially assessed on the raw broadband (0.1–100 Hz) signal. The measure that provided the best results in terms of distinguishing ASD from control participants at the individual level was further evaluated in the frequency domain, by separately computing indices in the delta (1–4 Hz), theta (5–7 Hz), alpha (8–13 Hz), beta (14–30 Hz), and gamma (30–90 Hz) frequency bands. Global as well as band-specific indices were used to determine the nature of group differences in sensor-level connectivity patterns. For the band-specific data we additionally calculated synchronization indices using coherence [32] for comparison. The computation of RIM, MI and PDC is described below. Additional computational information and detailed comparisons between synchronization measures can be found in [33,34].

2.1.1. Robust (non-linear) interdependence measure

Arnhold et al. [35] presented a measure for characterizing statistical relationships between two time series, which was later improved by Quian Quiroga et al. [36]. Given two scalar time series $\{x(t)\}_{t\in\mathbb{T}}$ and $\{y(t)\}_{t\in\mathbb{T}}$ with $\mathbb{T}=\{1,\ldots,T\}$, the dynamics of the hypothetical underlying systems X and Y, respectively, are estimated using delay coordinates [37]:

$$\mathbf{x}(t)=[x(t),x(t+\tau),\ldots,x(t+(d-1)\tau)]^T$$

In a similar fashion we reconstructed $\mathbf{y}(t)$ from $\{y(t)\}_{t\in\mathbb{T}}$, with an embedding dimension d and a delay time τ for $t\in\mathbb{T}'=\{1,\ldots,T'\}$, where $T'=T-(d-1)\tau$.

Let $r_{t,j}$ and $s_{t,j}$, $j=1,\ldots,k$, denote the time indices of the k nearest Euclidean neighbors of $\mathbf{x}(t)$ and $\mathbf{y}(t)$, respectively. Temporally correlated neighbors were excluded by means of a Theiler [38] correction: $|r_{t,j}-t|>d\cdot\tau$ and $|s_{t,j}-t|>d\cdot\tau$. For each $t\in\mathbb{T}'$, the average square distance of $\mathbf{y}(t)$ to all remaining points in $\{\mathbf{y}(j)\}_{j\in\mathbb{T}'}$ is given by

$$R_t(Y)=\frac{1}{T'-1}\sum_{j=1,j\neq t}^{T'}|\mathbf{y}(t)-\mathbf{y}(j)|^2$$

For each $\mathbf{y}_t$, the X-conditioned mean squared Euclidean distance is defined as

$$R_t^{(k)}(Y/X)=\frac{1}{k}\sum_{j=1}^{k}|\mathbf{y}(t)-\mathbf{y}(r_{t,j})|^2$$

Quian Quiroga et al. [36] defined the dependence measure:

$$N(Y/X)=\frac{1}{T'}\sum_{t=1}^{T'}\frac{R_t(Y)-R_t^{(k)}(Y/X)}{R_t(Y)} \quad (1)$$

The measure $N(X/Y)$ is defined in complete analogy. Although, in general: $N(X/Y)\neq N(Y/X)$, this measure is not suitable for inferring driver-response relationships [35]. For this reason, RIM values between X and Y were calculated as the mean of $N(X/Y)$ and $N(Y/X)$.

The parameters τ and d were selected using empirical and heuristic criteria [39]. Given a time series $\{x(t)\}$, parameter τ is the argument of the first local minimum in the mutual information between time series $\{x(t)\}$ and its delayed version $\{x(t+\tau)\}$ [40]. An algorithm to compute the mutual information between two finite time series is described in Section 2.1.2. Parameter d is determined using false nearest neighbor statistics [41]. After calculating the optimal parameters τ and d for every subject, segment and channel we selected $\tau=10$ and $d=14$ for all calculations of RIM. Note here that small variations in parameter τ have negligible effects in the reconstruction of the dynamics of a system. Similarly, the reconstruction is not very sensitive to parameter d provided that d is above some critical value which can be determined using the false nearest neighbor statistic.

Parameter k determines the size of the neighborhood of a delay vector $\mathbf{x}(t)$. A value of k between 10 and 30 is a reasonable choice given that the set of delay vectors, that can be paired with $\mathbf{x}(t)$, contains $T'-2*th=T-(d-1)*\tau-2*th=6102-13*10-2*14*10=5692$ elements, where th is the number of neighbor delay vectors of $\mathbf{x}(t)$ that are excluded since they are temporally correlated with $\mathbf{x}(t)$ (Theiler correction [38]). Usually $th\geq d\cdot\tau$. In this work th was set to $d\cdot\tau$ and k was set to 15.

2.1.2. Mutual information

While RIM is based on similarities in the time domain, *mutual information* (MI) measures the interdependence of two time series using an algorithm derived from information-theory concepts. Mutual information has several important advantages. First, it is sensitive to any type of dependence, including non-linear relations among the time series, such as the generalized synchronization (see Section 2.1.1). Second, it is relatively insensitive to outliers in measurement space and third, it is measured on a physically meaningful scale (bits when logarithms to the base 2 are used). The MI of two discrete random variables X and Y is defined as

$$I(X;Y)=\sum_{y\in Y}\sum_{x\in X}p(x,y)\log\left(\frac{p(x,y)}{p_x(x)\cdot p_y(y)}\right) \quad (2)$$

where $p(x,y)$ is the joint probability distribution function of X and Y, and $p_x(x)=\sum_{y\in Y}p(x,y)$ and $p_y(y)=\sum_{x\in X}p(x,y)$ are the marginal probability distribution functions of X and Y, respectively. In the case of continuous variables, the summation is replaced by a definite double integral.

Estimating MI for two finite time series $\{x(t)\}_{t\in\mathbb{T}}$ and $\{y(t)\}_{t\in\mathbb{T}}$ with $\mathbb{T}=\{1,\ldots,T\}$ is far from trivial since the distributions $p_x(x)$, $p_y(y)$ and $p(x,y)$ are unknown. The most straightforward approach for estimating MI consists of, first, discretizing the analog signals into a set of bins; then estimating the density functions $p_x(x)$, $p_y(y)$ and $p(x,y)$ by counting the number of points falling into the various bins. The *plug-in* estimate of MI is obtained by plugging the empirically derived discrete probabilities into (2). The alternative of naively identifying observed frequencies of events with probabilities leads to systematic errors and overestimation of MI. There is an extensive literature dealing with how to correct these errors [42–44]. For this reason, we have elected to estimate MI using the *direct method* of Strong et al. [43] which computes bias terms, as a function of sample size, directly from the data. In this approach, the bias terms are used to improve the plug-in estimate of MI. For an implementation of the direct method see [45]. Alternative MI estimation methods are reviewed by Hlaváčková–Schindler et al. [46].

2.1.3. Partial directed coherence (PDC)

In order to provide a frequency domain measure for Granger-causality, Baccalá and Sameshima [47] introduced the concept of

PDC. This measure was derived from a factorization of the partial spectral coherence and is based on the Fourier transform of the coefficient series of a vector autoregressive model of the time series.

Let $\{\mathbf{x}(t)\}_{t\in\mathbb{T}}$ with $\mathbf{x}(t)=[x_1(t),\ldots,x_n(t)]^T$ be a stationary n-dimensional time series with a mean of zero. Then a vector autoregressive model of order ρ for $\mathbf{x}$ is given by

$$\mathbf{x}(t)=\sum_{r=1}^{\rho}\mathbf{A}(r)\mathbf{x}(t-r)+\boldsymbol{\varepsilon}(t) \tag{3}$$

where $\mathbf{A}(r)$ are the $n\times n$ coefficient matrices of the model and $\boldsymbol{\varepsilon}(t)$ is a multivariate Gaussian white noise process with covariance matrix $\boldsymbol{\Sigma}$. In this model, the coefficients $A_{ij}(r)$ describe how the present values of x_i depend linearly on the past values of the components x_j.

Let

$$\overline{\mathbf{A}}(\omega)=I-\sum_{r=1}^{\rho}\mathbf{A}(r)e^{-i\omega r} \tag{4}$$

denote the difference between the n-dimensional identity matrix I and the Fourier transform of the coefficient matrices. Then the PDC from x_j to x_i is defined as

$$\pi_{i\leftarrow j}(\omega)=\frac{|\overline{A}_{ij}(\omega)|}{\sqrt{\sum_{l=1}^{n}|\overline{A}_{lj}(\omega)|^2}} \tag{5}$$

The PDC $\pi_{i\leftarrow j}(\omega)$ takes values between 0 and 1 and vanishes for all frequencies ω if and only if the coefficients $A_{ij}(r)$ are zero for all $r=1,\ldots,\rho$.

The model order ρ was chosen according to Akaike information criterion and in all cases it was a number between 22 and 28. Knowing the optimal value of ρ is not critical, since the results are not sensitive to small changes of ρ. For an implementation of PDC see [48].

2.2. Network modeling and visualization

A recent trend in brain functional connectivity analysis is to model the interdependencies among brain signals as networks [49,50,30]. Based on a particular measure of signal interdependence (such as RIM, MI, and PDC) one may then compute certain network statistics that characterize the network. On the basis of these calculated properties one can estimate the effects of subject-level variables (e.g., group membership) and of within-subject, task-related variables (such as cognitive load) on functional connectivity. Graph theory is perhaps the most widely used approach to network modeling.

2.2.1. Graph theoretical concepts

A *graph* $G=(V,E)$ is defined as a set of n *vertices* $V=\{v_1,\ldots,v_n\}$ and m *edges* $E=\{e_1,\ldots,e_m\}$. An edge $e\in E$ is a pair of vertices, which can be either ordered $e=(u,v)\in V\times V$ (known as a *directed edge*), or unordered $e=\{u,v\}$, where $u,v\in V$ (*undirected edge*). When $u=v$, e the pair is called a *self-loop*. Here we consider *simple* graphs, namely graphs without self-loops and multiple edges. Note that RIM, MI and the traditional coherence produce undirected simple graphs, while PDC produces directed simple graphs. An induced subgraph of G is one that consists of some of the vertices of G and all the edges that connect them. A *valued graph* or *valued network* $G=(V,E,\omega)$ is a graph comprising vertex set V and edge set E augmented with an edge value function $\omega: E\to\mathbb{R}$ that assigns a real value $\omega(e)$ to each edge $e\in E$. In this work we consider a particular type of valued networks, which we will call *synchronization networks*, where edges take values between 0 and 1 and serve as indices of the strength of the dependence between vertices.

In synchronization networks higher edge values indicate stronger dependencies. To define the length of an edge we may reverse the order of edge values by applying, for example, the function $\ell:(0,1]\to[1,+\infty)$ with equation [51]

$$\ell(x)=1-\log_2(x) \tag{6}$$

The length of a path from vertex u to vertex v is the sum of the lengths of the edges of the path. The shortest path distance from vertex u to vertex v is denoted by $d_G(u,v)$. If vertex v is unreachable from vertex u then $d_G(u,v)=+\infty$.

2.2.2. Network construction

Network modeling of the present data started by calculating interdependencies for each channel pair, separately for each subject, band (including the broadband signal) and synchronization measure. The results were stored to $n\times n$ synchronization matrices (where n is the number of selected channels) with elements ranging from 0 to 1. A synchronization matrix $W=[w_{ij}]$ corresponds to a synchronization network $G=(V,E,\omega)$ with vertex set $V=\{v_1,v_2,\ldots,v_n\}$, and edge set E defined by the non-zero elements of W, i.e., an edge $e=(v_i,v_j)$ between vertices v_i and v_j is included if and only if $w_{ij}>0$; the value of e is set to $\omega(e)=w_{ij}$.

2.2.3. Network measures

In order to characterize a network, it is necessary to reduce the information by describing its essential properties into a limited set of parameters (often called measures or metrics). Network measures are easily computable statistics which are chosen in such a way as to capture the relevant information necessary to differentiate computed networks into discrete classes, according to the goal and hypotheses of the study. Here we consider well-established network measures which have been introduced in previous research on complex and social networks as well as custom network metrics, by taking into account the general outline of brain regions expected to display reduced functional connectivity in ASD. Widely used global network measures implemented here include average strength, the clustering coefficient [52,53], the assortativity coefficient [54,55], and the global network efficiency index [56,57].

Average strength: In undirected networks, the strength $s(v)$ of a vertex $v\in V$ is defined as the sum of values of edges adjacent to v:

$$s(v)=\sum_{e=\{v,u\}\in E}\omega(e) \tag{7}$$

In directed networks one can define the in-strength $s^-(v)$ as the sum of values of edges that arrive to v, the out-strength $s^+(v)$ as the sum of values of edges that depart from v, and the strength of vertex v as the sum of the in-strength and out-strength of v:

$$s^-(v)=\sum_{e=(u,v)\in E}\omega(e) \tag{8}$$

$$s^+(v)=\sum_{e=(v,u)\in E}\omega(e) \tag{9}$$

$$s(v)=s^-(v)+s^+(v) \tag{10}$$

The average strength, $s(G)$, of a graph G is the average of $s(v)$ taken over all vertices. The average in-strength $s^-(G)$ and out-strength $s^+(G)$ of G are defined similarly.

Clustering coefficient: For a vertex v the clustering coefficient $c(v)$ assesses the connectivity within its immediate neighborhood. A definition for undirected networks that use matrix W was proposed by Zhang and Horvath [53]. It is the quotient of the total intensity of the triangles that contain vertex v divided by the total intensity of the dyads of edges incident to vertex v, where

the intensity of a triangle is the product of the values of its edges and the intensity of a dyad is the product of the values of its edges:

$$c(v) = \frac{1}{\max_{i,j}(w_{ij})} \cdot \frac{\sum_{i \neq j \in V\setminus\{v\}} w_{vi} w_{ij} w_{jv}}{\sum_{i \neq j \in V\setminus\{v\}} w_{vi} w_{jv}} \tag{11}$$

where $\max_{i,j}(w_{ij})$ is a normalizing factor.

In directed networks Fagiolo [58] distinguishes four basic scenarios for a given vertex v to be located in a triangle. By summing the intensities of all triangles of all these scenarios as well as the intensities of all dyads that contain vertex v we arrive at the following equation:

$$c(v) = \frac{1}{\max_{i,j}(w_{ij})} \cdot \frac{\sum_{i \neq j \in V\setminus\{v\}} (w_{vi}+w_{iv}) \cdot (w_{ij}+w_{ji}) \cdot (w_{vj}+w_{jv})}{2\sum_{i \neq j \in V\setminus\{v\}} (w_{vi}+w_{iv}) \cdot (w_{vj}+w_{jv})} \tag{12}$$

In both the directed and undirected cases the clustering coefficient $c(G)$ of a graph is the average of $c(v)$ taken over all vertices.

Assortativity: The assortativity coefficient was first defined by Newman [54] for undirected graphs. Leung and Chau [55] extended this definition to cover the class of undirected synchronization networks. We will further extend the definition of Leung and Chau to cover the class of directed networks as well.

Using the direction of edges we correlate a scalar quantity of the origin vertices with the same scalar quantity of the destination vertices. This scalar quantity, defined on vertices $g : V \to \mathbb{R}$, can be the strength $s(v)$, the in-strength $s^-(v)$, the out-strength $s^+(v)$, or something else. Suppose that $E = \{e_1, e_2, \ldots, e_m\}$ are the edges of a graph G and that we form the vectors $x = [g(orig(e_1)), \ldots, g(orig(e_m))]$ and $y = [g(dest(e_1)), \ldots, g(dest(e_m))]$, where $orig(e_i)$ and $dest(e_i)$ are the origin and destination vertices of edge e_i. Then the assortativity coefficient is the weighted Pearson correlation, $\mathrm{corr}(x,y)$, of vector x and y with weights the edge values. After some calculations we arrive at the following equation:

$$r(G) = \frac{H\sum_{(u,v) \in E} \omega(u,v) g(u) g(v) - AB}{\sqrt{H\sum_{(u,v) \in E} \omega(u,v) g(u)^2 - A^2}\sqrt{H\sum_{(u,v) \in E} \omega(u,v) g(v)^2 - B^2}} \tag{13}$$

where $A = \sum_{(u,v) \in E} \omega(u,v) g(u)$, $B = \sum_{(u,v) \in E} \omega(u,v) g(v)$ and $H = \sum_{e \in E} \omega(e)$ is the sum of all values of edges in E.

Note that in undirected graphs (13) reduces to the equation proposed by Leung and Chau [55] if we substitute each undirected edge $\{u,v\}$ with two directed edges (u,v), (v,u) and if we set g equal to strength s. Also (13) generalizes the equations proposed by Piraveenan et al. [59].

The assortativity coefficient measures whether a network is optimized for easy transfer of information in which case the network is assortative ($r > 0$) or for robustness, in which case the network is disassortative ($r < 0$). Park et al. [60] report that typically functional brain networks are assortative.

Efficiency: For a vertex v Latora and Marchiori [56] defined efficiency as

$$ef(v) = \frac{1}{n-1} \sum_{u \neq v} \frac{1}{d_G(v,u)} \tag{14}$$

Note that (14) can also be used for disconnected graphs. If some vertices v and u are not connected then they do not contribute to $ef(v)$. In this case, $d_G(v,u) = +\infty \Rightarrow 1/d_G(v,u) = 0$. The global efficiency, $ef(G)$, of a graph is the average of $ef(v)$ taken over all vertices. The definitions of vertex efficiency and of global network efficiency apply both to directed and undirected networks.

Within- and between-sector strength: The network measures mentioned above were developed for general complex networks and may not optimally differentiate ASD and control participants, as they do not take into account the spatial distribution of sensors in relation to potentially important underlying activity sources. In order to provide more suitable indices of connectivity we adopted a region of interest approach and we introduced two sets of metrics that accumulate edge values either within or between specific sectors of the sensor array. Within-sector strength measures accumulate the edge values of the edges within each predefined sector of the sensor array (see Fig. 2). Seven within-sector metrics were defined, $S_W(i)$, $i \in \{1, \ldots, 7\}$ (see (15); the eighth sector consisted of a single occipital sensor and was thus not included in the within-sector measure calculations), using the formula:

$$S_W(i) = \sum_{e \in E_i} \omega(e) \tag{15}$$

where E_i are the edges of the subgraph G_i of G "connecting" the vertices of sector L_i, $i \in \{1, \ldots, 7\}$.

Conversely, each of the between-sector strength measures accumulated the values of the edges formed by the sensors of a

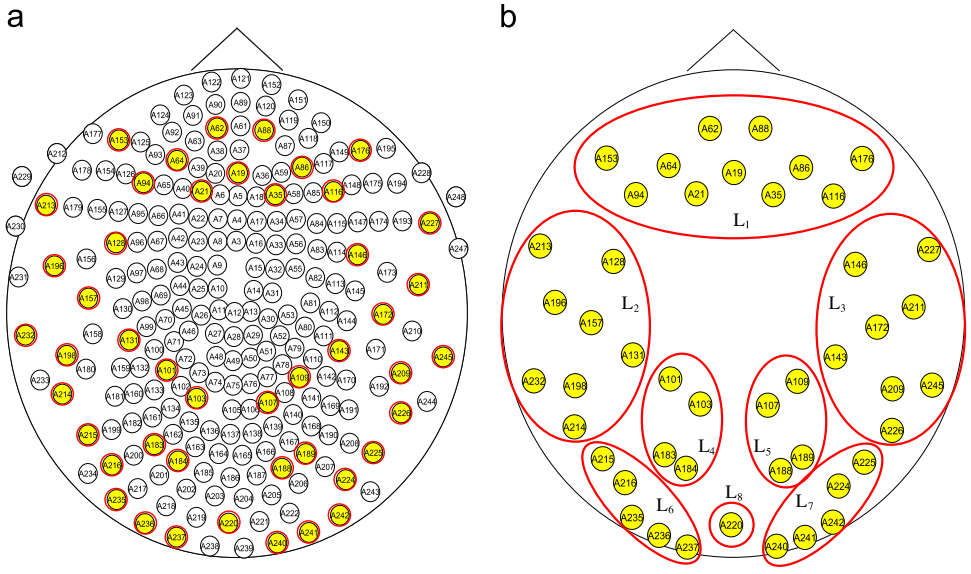

Fig. 2. (a) Spatial layout of all MEG sensors and of the selected 46 sensors. Nine sensors with excessive noise are not shown. (b) Elliptic shapes indicate sensor sectors labeled L1–L8.

particular sector with the sensors comprising all the remaining sectors. Between-sector metrics, $S_B(i)$, $i \in \{1,\ldots,8\}$ (see (16)), were computed for each of the eight sectors:

$$S_B(i) = \sum_{j \neq i \{u,v\} \in E,\ u \in V_i,\ v \in V_j} \omega(e) \tag{16}$$

where V_i and V_j are the vertices of sectors L_i and L_j, respectively, with $i \in \{1,\ldots,8\}$, and $j \in \{1,\ldots,8\} \backslash \{i\}$ spans the other sectors L_j.

For example, $S_B(1)$ accumulates the edge values between the sensors of the bilateral frontal sector (L_1) and the sensors of all other sectors: left and right temporal (L_2 and L_3), left and right parietal (L_4 and L_5), left and right ventral occipitotemporal (L_6 and L_7) and midline occipital (L_8).

2.2.4. Analytic strategy

The potential utility of connectivity estimates as biomarkers of ASD was examined by performing leave-one-out cross-validation classification analyses. In this technique a classifier, in this case a support vector machine with a linear kernel, was trained using the data from all but one subjects from both groups and its generalization performance was tested with the remaining subject. The procedure was repeated such that every subject's network parameters served once as the validation data set. At the end of each set of cross-validation analyses we estimated the sensitivity, specificity and accuracy of the measure that served as the classification feature. Sensitivity focuses on the proportion of true positives (i.e., correctly identified ASD participants), specificity primarily concerns the proportion of true negatives (i.e., correctly identified control participants), and accuracy is the proportion of correctly identified participants. Classification runs were performed separately for each graph measure (average strength, clustering coefficient, assortativity coefficient, efficiency, within- and between-sector strength indices) and for each measure of interdependence (RIM, MI, PDC and coherence). Thus the total number of cross-validation sets for individual features is (1 [for the broadband signal] + the number of frequency bands in which the signal is filtered) $\times$ (number of interdependence measures) $\times$ (number of graph measures) $= (1 + 5) \times 4 \times (4 + 15) = 456$ sets of tests. Additionally, cross-validation tests were performed with composite features (i.e., features that consist of two or more graph measures). Namely, for each measure of connectivity (RIM, MI, PDC and coherence) and frequency band we chose the five best graph measures and we formed all possible combinations of two and three graph measures. Therefore the total number of cross-validation sets of tests that were performed with composite features were $4 \times 6 \times (\binom{5}{2} + \binom{5}{3}) = 480$.

In addition, the direction of group differences on each of the four global graph measures (clustering, assortativity, efficiency, and strength) was assessed through multivariate one-way ANOVAs with Group as the between subjects variable. Supplementary, parametric analyses assessed the spatial distribution and spectral specificity of group differences on the custom graph indices. A separate ANOVA was carried out on the indices derived from each interdependence measure (RIM, MI, and PDC), with sector as the within subjects variable (with eight levels for the between-sector data and seven levels for the within-sector data) and group (2) as the between subjects variable. Significant two-way interactions were further explored by assessing group simple main effects at each sector.

2.2.5. Network visualization

Network visualization is useful in order to describe the hidden structure of a network graphically and renders potential group differences more apparent. Visualizing all edges of a "dense" valued network might lead to an unintelligible image. For this reason sensor-level networks were visualized by first converting the set of continuous graph parameters for each participant into a "binary" graph which contained only a selected subset of the edges of the original network;namely only the strongest edges. The new graph included edges $e=(v_i,v_j)$ if and only if $\omega(e) = w_{ij} \geq \theta$, where θ is a user-selected threshold. For PDC data, the threshold was set so that $\theta \geq \max_{v_i,v_j \in V} w'_{ij}$, where w'_{ij} is the significance level of the hypothesis that the PDC from v_j to v_i is zero (H_0: $\pi_{i \leftarrow j}(\omega) = 0$) [61,62]. For RIM and MI data, the threshold was set so that $\theta \geq \max_{v_i,v_j \in V}(\langle w'_{ij} \rangle + 1.645 * \sigma_{w'_{ij}})$, where $\langle w'_{ij} \rangle$ is the average value and $\sigma_{w'_{ij}}$ is the standard deviation across 30 repetitions of calculations of surrogate synchronization between v_i and v_j. To calculate surrogate synchronization between time series $\{x_i(t)\}$ and $\{x_j(t)\}$ we randomly shuffled (i.e., re-ordered) $\{x_j(t)\}$, in order to minimize dependencies between $\{x_i(t)\}$ and $\{x_j(t)\}$, and then we calculated RIM and MI on the rearranged time series [63]. The vertices of this binary graph were assigned the coordinates of the corresponding channels.

In addition to outlining the group-average layout of the sensor-level, resting-state network for each group, it is informative to visualize the differences between the networks for the two groups of participants. It is of particular interest to identify edges that were stronger (or weaker) for controls than ASD participants (see Fig. 4). We identified these edges as follows. Let $W(q)$ be the synchronization matrix of subject q and $w_{ij}(q)$ be its (i,j) element. We remind the reader here that when $w_{ij}(q) > 0$ then $w_{ij}(q)$ is the value of edge (v_i,v_j) from vertex v_i to vertex v_j. For each $i,j \in \{1,\ldots,n\}$, $i \neq j$ we sorted in descending order the elements $w_{ij}(q)$, for all subjects. If the majority of the first half of the sorted elements corresponded to control subjects we identified edge (v_i,v_j) as being stronger in the control than in the ASD group. Conversely if the majority of the sorted elements characterized ASD subjects we identified edge (v_i,v_j) as being stronger in the ASD than in the control group. Edges (v_i,v_j) that did not meet these criteria were not displayed. While it may be striking that isolated edges perfectly discriminated participants in the two groups, they were not considered further given that single edges are not likely to constitute robust features for subject classification.

3. Application

3.1. Participants

Recruitment criteria for individuals with autism and matched controls have been described previously [64]. The primary target group consisted of eight young adults who had been diagnosed with high-functioning autism using the autism diagnostic observation schedule [65] and the autism diagnostic interview, revised [66]. The control group consisted of eight young adults with unremarkable neurological and psychiatric history. For both control and high-functioning autism participants, a full-scale IQ (FSIQ) index was derived from the verbal (VIQ) and performance

Table 1
Demographic and IQ information on the two groups of participants. FSIQ refers to an average of subtests of vocabulary and of pattern analysis/nonverbal reasoning. Scores of the autism screening questionnaire (ASQ)/social communication questionnaire (SCQ) are also shown. Groups differ at level: $^*p < 0.01$.

	Controls ($n = 8$)	ASD ($n=8$)
Gender (boys/girls)	7/1	7/1
Age (years)	20.1 ± 4.9 (17–21)	18.9 ± 2.6 (17–20)
FSIQ*	126.6 ± 8.4 (116–139)	104.6 ± 15.8 (85–125)
VIQ	122.7 ± 8.0 (116–136)	101.6 ± 16.8 (73–122)
PIQ	122.6 ± 5.6 (116–132)	107.0 ± 14.2 (83–126)
ASQ (SCQ)	–	20.70 ± 6.7 (18–28)

(PIQ) IQ scales of the Wechsler abbreviated scales of intelligence [67]. In the present sample, participants with high-functioning autism had lower estimated full-scale IQ scores than typically developing individuals (see Table 1). On average controls were slightly older than ASD participants although the age range in the two groups was identical. Written informed consent was obtained from all subjects according to institutional review boards for the protection of human research participants at the University of Houston and University of Texas Health Science Center-Houston.

3.2. MEG data acquisition

Magnetic recordings were performed with a whole-head neuromagnetometer (4D Neuroimaging; San Diego, CA) equipped with 248 axial gradiometer sensors and housed in a magnetically shielded room designed to reduce environmental magnetic noise. The recording sessions required the participants to lie as still as possible with their eyes closed; on a bed with their head inside the helmet-like device. The entire experimental session lasted approximately 30 min per participant, and included 20 min for head digitization and subject acclimation. Ongoing activity was acquired in a single time series record for 3 min. The recorded signals were filtered online with a band pass between 0.1 and 100 Hz and digitized at a rate of 1017 Hz. For the task of noise reduction the 3 min time series was split into 90 2-s segments and each was inspected for muscle and sensor jump artifacts. Segments with excessive artifacts were rejected and the remaining segments were concatenated to form a single segment. For uniformity, 150 s of recording ($150 \times 1017 = 152{,}550$ samples) was retained for each subject. Nine MEG channels presenting extreme variance values were identified and excluded from further processing. Finally, a set of 46 channels which were deemed representative of eight major helmet sectors (roughly corresponding to bilateral frontal, occipital, left and right temporal, parietal, and ventral occipitotemporal placements) were selected to form a synchronization network (see Fig. 2). The small number of selected channels dramatically reduced processing time and computer memory requirements of the interdependence measures without significantly affecting the differentiation between the networks of ASD and control subjects (compare Tables 2 and 6).

3.3. Results

As shown in Fig. 3 the networks derived from RIM and MI appeared very similar to each other and both had "long" edges spanning distant sensor array sectors. Conversely, the networks resulting from PDC were composed mainly of "short" edges. Fig. 3 is particularly revealing of the scarcity of "long" range connections among ASD participants, in accordance with the disconnection hypothesis of autism [15] and with the work of Monk et al. [23].

The results of the leave-one-out classification analyses are presented in Tables 2, 4 and 5 for each graph measure. Sensitivity and specificity estimates permit comparisons of the relative classification efficiency across the three measures of signal interdependence from which graph network measures were derived. Thus, it becomes apparent that hypothetical networks calculated from RIM measures of interdependence contain more information relevant to group differences than networks computed with MI. Additionally, PDC is inferior to both RIM and MI in differentiating ASD from typically developing participants. Fig. 4 helps to identify the edges that differentiate ASD from control participants based on RIM-derived graph measures. Attenuated short-range "connections" in ASD participants were found within bilateral "temporal" and "frontal" sectors as well as within the left parietal sector. Moreover, practically all "connections" formed by the sets of "temporal" and "frontal" sensors with other sensors were attenuated among ASD participants. Statistical evaluations of these apparent group differences are reported below.

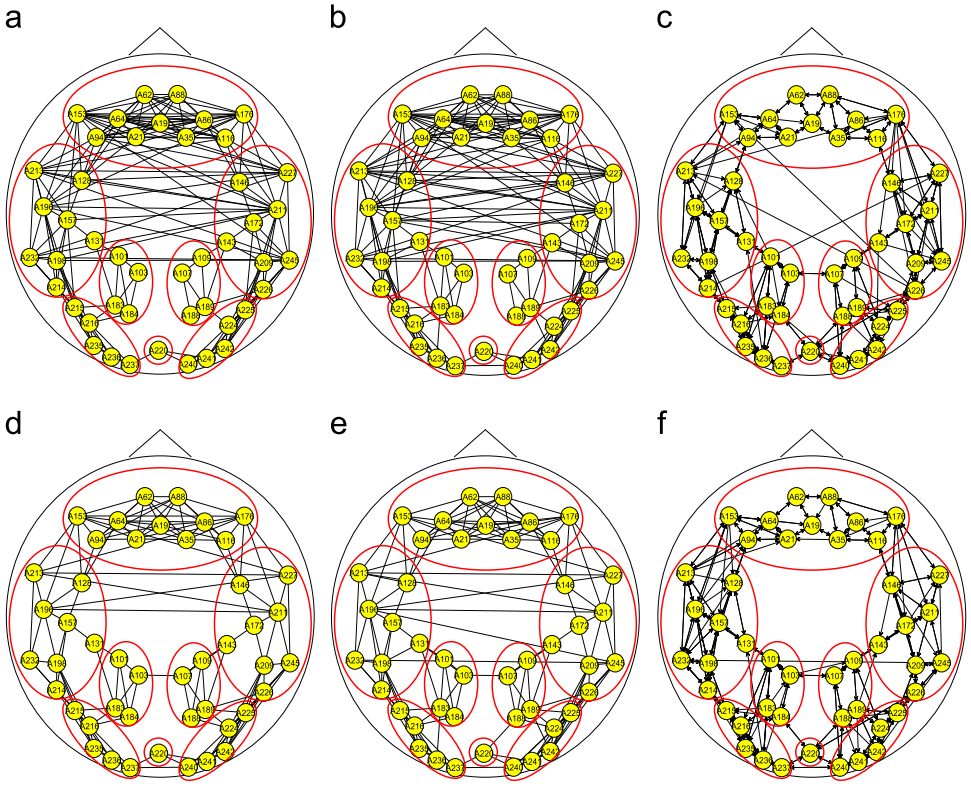

Fig. 3. (a–c) Average resting-state functional network across typically developing participants ($n = 8$). (d–f) Average resting-state functional network for the ASD group ($n = 8$). The networks were calculated using (a and d) RIM, (b and e) MI, (c and f) PDC.

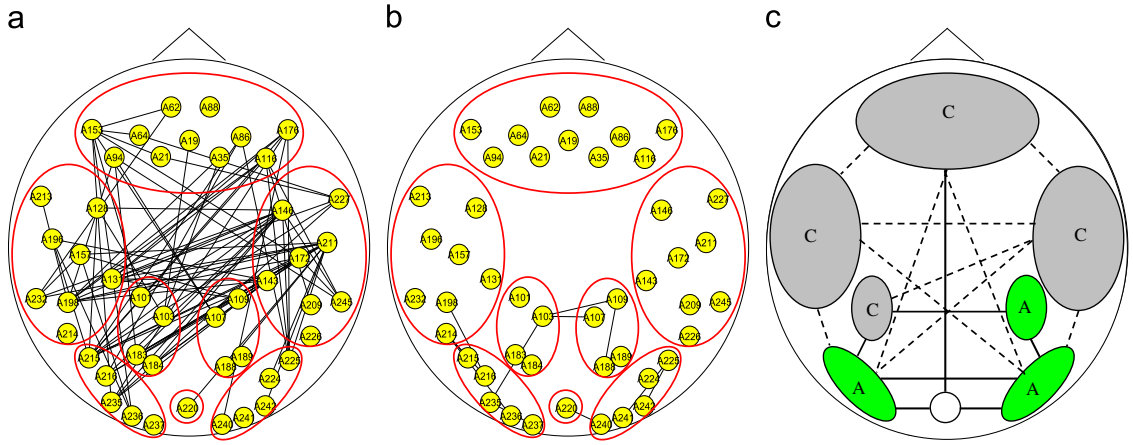

Fig. 4. Hypothetical network differences between control and ASD participants. Networks were estimated by RIM. (a) Solid lines represent edges which were stronger for the majority of controls compared to the majority of ASD participants. (b) Solid lines represent edges which were stronger for the majority of ASD participants as compared to the majority of controls. (c) Schematic rendering of "connections" between-sectors. The dashed lines depict stronger connections for controls, while the solid lines depict stronger connections for ASD participants. Sectors with stronger intrinsic connections for controls are labeled by C, while sectors with stronger intrinsic connections for ASD participants are labeled by A.

Table 2
Classification results using graph measures as features. The networks were calculated using RIM in the broadband MEG signal. $S_B(1)$, $S_B(2)$ and $S_B(3)$ are the between-sector strength metrics for bilateral frontal, left and right temporal sectors, respectively. $S_W(3)$ indicates average within-sector strength for the right temporal sector.

Feature(s)	True positives	True negatives	Sensitivity (%)	Specificity (%)
Average strength	7	6	87.5	75
Clustering coefficient	6	4	75	50
Assortativity coefficient	5	4	62.5	50
Efficiency	7	6	87.5	75
$S_W(3)$	7	7	87.5	87.5
$S_B(1)$	7	6	87.5	75
$S_B(2)$	7	7	87.5	87.5
$S_B(3)$	7	7	87.5	87.5
$\{S_W(3),S_B(2),S_B(3)\}$	8	7	100	87.5

Table 3
Classification results using graph measures as features. Networks were calculated using RIM in the alpha band.

Feature(s)	True positives	True negatives	Sensitivity (%)	Specificity (%)
Average strength	7	5	87.5	62.5
Clustering coefficient	6	5	75	62.5
Assortativity coefficient	6	6	75	75
Efficiency	7	5	87.5	62.5
$S_W(3)$	6	6	75	75
$S_B(1)$	6	5	75	62.5
$S_B(2)$	6	6	75	75
$S_B(3)$	5	6	62.5	75
$\{S_W(3),S_B(2),S_B(3)\}$	6	6	75	75

Table 4
Classification results using network measures as features. Networks were calculated using MI in the broadband MEG signal.

Feature(s)	True positives	True negatives	Sensitivity (%)	Specificity (%)
Average strength	6	6	75	75
Clustering coefficient	6	5	75	62.5
Assortativity coefficient	4	3	50	37.5
Efficiency	5	4	62.5	50
$S_W(3)$	6	5	75	62.5
$S_B(1)$	7	6	87.5	75
$S_B(2)$	7	5	87.5	62.5
$S_B(3)$	7	6	87.5	75
$\{S_W(3),S_B(2),S_B(3)\}$	7	6	87.5	75

Inspection of Table 2 further suggests that the assortativity coefficient may not be an appropriate feature for individual subject classification. Note here that all functional networks that we computed are assortative as expected. Neither clustering coefficient, which measures the local connectivity of a network, can be considered as a strong biomarker of autism. Classification results may be considered satisfactory using the global efficiency index, which takes into account the global structure of the network and if used as a single feature led to 13/16=81.25% accuracy. Similar results were achieved by using average strength. However, the highest accuracy, 14/16=87.5%, was achieved by one within- and two between-sector graph metrics. These metrics reflected the average strength of the edges formed within the right "temporal" sector $S_W(3)$, and also the average strength of the edges formed by each of the left $S_B(2)$ and right "temporal" sectors $S_B(3)$ with all the remaining sensors. Note also that the combination of the three parameters $S_W(3)$, $S_B(2)$, $S_B(3)$ led to 15/16=93.75% classification accuracy.

By comparing Tables 2 and 3 it is apparent that classification accuracy was higher in the broadband signal than in the alpha band. Classification accuracy was also higher in the alpha band than in the delta, theta, beta and gamma bands. These results hold for all synchronization measures employed (RIM, MI, PDC and coherence).

3.3.1. Group differences in connectivity

This section describes the results of parametric analyses performed on the global graph parameters (strength, assortativity, clustering, and efficiency), as well as on the spatially constrained graph indices (within- and between-sector average strength)

Table 5
Classification results using network measures as features. Networks were calculated using PDC in the broadband MEG signal.

Feature(s)	True positives	True negatives	Sensitivity (%)	Specificity (%)
Average strength	3	3	37.5	37.5
Clustering coefficient	4	5	50	62.5
Assortativity coefficient	6	6	75	75
Efficiency	4	3	50	37.5
$S_W(3)$	6	5	75	62.5
$S_B(1)$	6	6	75	75
$S_B(2)$	3	3	37.5	37.5
$S_B(3)$	7	4	87.5	50
$\{S_W(3),S_B(2),S_B(3)\}$	7	5	87.5	62.5

Table 6
Classification results using graph measures as features. The networks were calculated using RIM on broadband MEG signals from 239 channels (248 channels minus 9 channels with excessive noise). Compare with Table 2 where only the 46 channels shown in Fig. 2 were used.

Feature(s)	True positives	True negatives	Sensitivity (%)	Specificity (%)
Average strength	7	6	87.5	75
Clustering coefficient	6	3	75	37.5
Assortativity coefficient	5	3	62.5	37.5
Efficiency	7	6	87.5	75
$S_W(3)$	8	6	100	75
$S_B(1)$	8	6	100	75
$S_B(2)$	8	6	100	75
$S_B(3)$	7	6	87.5	75
$\{S_W(3),S_B(2),S_B(3)\}$	8	6	100	75

estimated with RIM, MI, and PDC on the broadband MEG signal. Analyses on spatially tailored graph measures assessed the spatial layout of group differences in signal interdependencies. In general, ANOVA results corroborated the classification findings by documenting that the most reliable differences between groups (in all cases indicating reduced connectivity for ASD participants) occurred for connectivity estimates derived from RIM measures. For global graph-based parameters, group differences (NI > ASD) that met the Bonferroni-adjusted criterion of significance ($a=0.05/12=0.004$) were restricted to the global efficiency and strength measures derived from RIM indices. A non-significant trend in the same direction was noted for the RIM-derived clustering index ($p=0.01$).

For the spatially tailored average strength measures, group by sector interactions was found for the RIM-based between-sector measures: $F(2,26)=9.86$, $p=0.001$, and the RIM-based within sector measures: $F(2,26)=9.75$, $p=0.001$. Follow up one-way ANOVAs revealed that marginally significant group differences (NI > ASD) were restricted to the temporal sector, bilaterally ($p=0.003$) in both cases; Bonferroni-adjusted nominal alpha levels were set to $a=0.05/24=0.002$ for each family of comparisons. Non-significant trends in the same direction were noted for MI measures, but failed to reach the Bonferroni-adjusted alpha level for the omnibus ANOVA. There were no significant effects involving group for any of the PDC estimates.

Band-specific analyses on the RIM-derived indices indicated that group differences were restricted to the alpha band. Interestingly, the traditional magnitude square coherence measure (MSC) [32] only revealed non-significant trends (NI > ASD: $p<0.05$) for synchronization between bilateral temporal and the remaining sensors in the alpha band.

4. Discussion

The ultimate goal of this exploratory study was to identify features of hypothetical networks of resting neuromagnetic activity, modeled at the sensor-level, that reliably differentiate young adults with ASD from typically developing individuals. An additional self-imposed restriction on the analytical strategy concerned limiting computational resources in pursuing this goal. Measures of neuromagnetic signal interdependence were obtained at the sensor-level, in order to bypass the problems posed by the indeterminacy of the inverse problem in estimating source density distributions. Moreover, the results of source-level network modeling of resting activity, as opposed to stimulus-evoked activity reflecting the engagement of a particular brain mechanism, may not be readily interpretable in the same context. A secondary goal of the study was to spatially map network features that differentiated the two groups, in the form of short interconnecting paths within predefined sets of sensors, and also in the form of longer paths "connecting" sensors in one such set (sector) with sensors in other sets. In interpreting network visualizations such as those depicted in Fig. 4, one should bear in mind that these sensor-level representations, especially when derived from axial gradiometer recordings, are but rough approximations to the underlying network of regions that show synchronized neuronal signaling at rest.

In our study we selected a set of 46 channels, as representative of eight major helmet sectors (roughly corresponding to bilateral frontal, occipital, left and right temporal, parietal, and ventral occipitotemporal placements), to form a synchronization network. This strategy had two consequences: (a) it reduced the computation requirements for the synchronization measures (time and memory) and (b) it filtered out most of the "short" edges which are common to autistic and control subjects and appear as noise for the classification task. By removing a vertex, we remove the connections of this vertex with its immediate geographical neighbors. Note that we also lose some "long" connections. By systematically removing vertices we filter out most of the "short" edges and make the remaining "long" edges more discernible. Importantly, however, classification results were very similar when using the entire sensor array (and only excluding few sensors containing excessive noise).

Given the small sample of the present study, the relative efficiency of each feature was assessed though a series of leave-one-out classification analyzes. Initially, interdependence measures were calculated on the broadband (0.1–100 Hz) signal. Results clearly showed that network features based on RIM outperformed corresponding measures derived from sensor interdependencies estimated using PDC in differentiating between the two groups. PDC was initially considered as a measure because of its purported sensitivity to direct causal interactions and of its multivariate nature. The fact that PDC-derived networks were dominated by "short" edges may have contributed to the poor classification outcome. Whether this feature of PDC-derived network models is characteristic to the technique in general or reflects a peculiarity of applying this algorithm to axial gradiometer MEG data is an issue that requires extensive simulation modeling to address. RIM was also slightly superior to MI in maximizing group-specific network features and has the added advantage of requiring fewer computational resources.

The best classification results were obtained for a spatially constrained graph parameter (average strength of edges) based on RIM interdependence estimates, as compared to the estimates of global graph characteristics (strength, clustering, assortativity, and efficiency across the entire set of 46 sensors). Three of the custom connectivity indices produced optimal, yet comparable to each other, classification results: average interdependence within

the set of right "temporal" sensors, average interdependence between all the right "temporal" sensors and the remaining sensors (in the "frontal", left "temporal", left and right "parietal", left and right "ventral occipital", and midline "occipital" sectors), and average interdependence between all the left "temporal" sensors and the remaining sensors. Further, by combining these measures (using them concurrently as classification features) we obtained the best classification rates reflecting 100% sensitivity and 87% specificity (only one control participant was misclassified). Group-level analyses, using stringent criteria for statistical significance, confirmed that the most reliable differences between ASD participants and controls concerned the strength of interactions between sensors located over temporal brain areas as well as the strength of interactions between bilateral "temporal" and the remaining preselected sensors (i.e., sensors over frontal, parietal, occipital, and occipitotemporal regions).

These analyses were repeated on band-limited data (in the delta, theta, alpha, beta, and gamma bands). Whereas classification results were clearly poorer for corresponding network features in each band, group-level parametric analyses indicated that RIM and MI measures produced networks that significantly differed between the two groups only in the alpha band. Interestingly, traditional coherence measures did not significantly differentiate the two groups (in group-level analyses). A preponderance of non-linear signal synchronization between sensors may have contributed to this outcome. This factor may have also affected the sensitivity of PDC-derived network measures.

The present results documenting a spatially specific pattern of sensor-level interactions are consistent with the results of two recent EEG studies on ASD. In the earlier study, Murias et al. [25] reported reduced alpha coherence between posterior and anterior regions on the basis of resting EEG data for a group of adult ASD participants compared to age-matched controls. More recently, Coben et al. [26] found reduced coherence between frontal and temporal regions for the group of ASD individuals as compared to the control group. Taken together, these findings utilizing resting-state recordings suggest that aberrant features of brain organization may be time-invariant, trait-specific markers in ASD.

Although not directly comparable, our findings are also consistent with an increasing number of neuroimaging studies linking ASD with disturbances in white matter integrity [11–13], especially increased fractional anisotropy values in the temporal lobes. Neuromagnetic studies during tasks requiring sensory processing also point to a functional deficit in the temporal lobes in ASD. Wilson et al. [68] reported that the 40 Hz steady-state auditory gamma power is reduced over the left hemisphere in individuals with ASD, suggesting a lack of coherent neuronal interactions. However, other studies have demonstrated that the cortical auditory processing abnormalities in ASD may be related to dysfunction of auditory processes in the right hemisphere. For example, children with ASD show reduced dynamic response range to frequency modulated stimuli in the right hemisphere [69] and the latency of the early component of the auditory magnetic evoked response (M100) in the right hemisphere deviates sufficiently from the normal range to function as a marker of ASD with a positive predictive value of 86% [70]. Moreover, two studies suggest that children with ASD do not exhibit the expected reduction in latency of the M100 that comes with age with one study implicating both the left and right hemispheres [69] and another study finding this phenomenon only in the right hemisphere [70].

A number of factors preclude direct comparisons of our results with previous fMRI findings. First, signal interdependencies were assessed at the sensor and not at the source level, a necessary condition in order to make statements regarding patterns of cortico-cortical functional connections. Second, interdependency metrics took into account rapid fluctuations in cortical activity, as opposed to more steady-state variations in blood-flow/regional oxygenation patterns. Third, our approach in defining networks does not coincide with the approach of other authors. For example, Kennedy and Courchesne [22] computed the connectivity between each of three regions (rostral mesial frontal, left angular, posterior cingulate) and the remaining brain. So they computed only a small subset of the network edges. Also, their indices of connectivity include both within and between-hemisphere voxel correlations. On the other hand we used a hypothesis-free approach where we looked at interdependencies between eight broad surface regions and we found reduced values between frontal and parieto-temporal sensors both within and between hemispheres. So although our results are not directly comparable to theirs, they are not inconsistent either. Therefore our findings should be considered as an initial attempt to establish computational methods aimed at deriving relatively stable surface-level patterns of activity that may prove to be characteristic of resting-state brain function in ASD. It is certainly encouraging that our results with respect to the regional pattern of reduced connectivity are generally consistent with previous resting-state fMRI findings although the exact structure of a synchronization network between MEG sensors depends on the distribution of the magnetic flux on the sensors and is certainly different from the structure of the corresponding synchronization network computed from fMRI data.

The present results are generally consistent with findings from two recent MEG studies employing more elaborate indices of signal interdependency than traditional coherence measures. Georgopoulos et al. [29] computed functional connectivity networks based on the entire array of 248 MEG sensors. The degree of synchronization within pairs of channels was computed using cross-correlation, from the residuals of an autoregressive integrative moving average (ARIMA) model. Then, they applied genetic algorithms to identify successful predictor subsets from the very large space of edges within the resulting synchronization network ($248 \times 247/2 = 30{,}628$). Weighted linear sums of Fisher's z-transform of the values of this subset of edges served as classification features, obtaining excellent classification results. Note that Georgopoulos et al. [29] also used valued graphs in their analysis. Pollonini et al. [71] also computed functional connectivity networks using all 248 channels of the MEG sensor array. They modeled each MEG signal with a vector autoregressive model and estimated Granger causality from the coefficients of the model. Then, for each subject, a binary network was constructed which included only the strongest links exceeding a prespecified threshold. Finally, the network structure that was common to both groups (ASD and controls) was subtracted to enhance group differences. The authors reported 87.5% classification accuracy using as features a set of 17 binary graph measures plus the values of a small subset (5–70) of the directed edges of a connectivity matrix. In their analysis they used both valued graphs and binary graphs. It should be noted that Granger causality is very similar to PDC, which corresponds to Granger causality computed in the frequency domain and derived from the coefficients of a vector autoregressive model of the MEG signal. For this reason one may expect Granger causality to show reduced sensitivity in differentiating between ASD participants and controls making necessary the inclusion of a relatively large set of (21) features to achieve 87.5% classification accuracy. Although sample sizes are small to permit reliable comparison between methods on classification accuracy, the existing data suggest that the method used by Georgopoulos et al. [29] may lead to higher classification performance. This may be attributed: (a) to the signal processing method used to construct functional connectivity networks, (b) to the larger set of sensors included in the analyses and (c) to the use of single edges as classification

features. A data set comprising 248 MEG channels produces networks with 30,628 edges, therefore increasing the likelihood of overfitting (because by mere chance some edges will be stronger in participants of one group than in those of the other group). Note that by considering the edges that perfectly separate the two groups as classification features we achieved 100% accuracy (see Section 2.2.5). Considering graph measures that average across many edges (such as the between- and within-sector graph measures) may reduce the risk of overfitting the data, producing more robust features than single edges. Such measures are more likely to represent inherent electrophysiological characteristics of ASD. Moreover they can easily be applied to virtually all existing synchronization measures that have been proposed in the literature.

Future studies should extend analyses to larger data sets, experiment with novel synchronization measures, consider more than two groups of patients concurrently, and use all channels in the synchronization networks in order to exploit all available information in the recorded data sets.

5. Summary

The present study is a preliminary attempt to use graph theory for deriving distinct features of resting-state functional networks in young adults with autism spectrum disorder (ASD). Networks modeled neuromagnetic signal interactions between sensors using three alternative interdependence measures: (a) a non-linear measure of generalized synchronization (robust interdependence measure (RIM)), (b) mutual information (MI), and (c) partial directed coherence (PDC). To summarize the information contained in each network model we employed well-established global graph measures (average strength, assortativity, clustering, and efficiency) as well as graph measures (average strength of edges) tailored to specific hypotheses concerning the spatial distribution of abnormalities in connectivity among individuals with ASD. Graph measures then served as features in leave-one-out classification analyses contrasting control and ASD participants. The best classification results were obtained for spatially constrained graph measures as compared to the estimates of global graph measures. With respect to the synchronization measure, used to construct the networks, RIM has higher sensitivity than MI and PDC in differentiating between autistic and control subjects. The above analyses refer to broadband MEG signal. For the band-specific data we additionally calculated synchronization indices using the traditional coherence for comparison. However, the band-limited data (in the delta, theta, alpha, beta, and gamma bands) did not lead to better classification results. There were significant trends for synchronization between bilateral temporal and the remaining sensors in the alpha band for networks calculated with RIM and MI. Interestingly, the traditional magnitude square coherence measure (MSC) only revealed non-significant trends for synchronization between bilateral temporal and the remaining sensors in the alpha band. In summary we found that combinations of regionally constrained graph measures, derived from RIM in the broadband signal, performed best, discriminating between the two groups with 93.75% accuracy. Network visualization revealed that ASD participants displayed significantly reduced interdependence strength, both within bilateral frontal and temporal sensors, as well as between temporal sensors and the remaining recording sites, in agreement with previous studies of functional connectivity in this disorder.

Conflict of interest statement

None declared.

References

[1] I. Rapin, M. Dunn, Update on the language disorders of individuals on the autistic spectrum, Brain and Development 25 (3) (2003) 166–172.
[2] M.K. Belmonte, G. Allen, A. Beckel-Mitchener, L.M. Boulanger, R.A. Carper, S.J. Webb, Autism and abnormal development of brain connectivity, The Journal of Neuroscience 24 (42) (2004) 9228–9231.
[3] E.L. Hill, Executive dysfunction in autism, Trends in Cognitive Sciences 8 (1) (2004) 26–32.
[4] G.M. McAlonan, V. Cheung, C. Cheung, J. Suckling, G.Y. Lam, K.S. Tai, L. Yip, D.G.M. Murphy, S.E. Chua, Mapping the brain in autism. A voxel-based MRI study of volumetric differences and intercorrelations in autism, Brain 128 (2) (2005) 268–276.
[5] E. Courchesne, C.M. Karns, H.R. Davis, R. Ziccardi, R.A. Carper, Z.D. Tigue, H.J. Chisum, P. Moses, K. Pierce, C. Lord, A.J. Lincoln, S. Pizzo, L. Schreibman, R.H. Haas, N.A. Akshoomoff, R.Y. Courchesne, Unusual brain growth patterns in early life in patients with autistic disorder, Neurology 57 (2001) 245–254.
[6] A.C. Stanfield, A.M. McIntosh, M.D. Spencer, R. Philip, S. Gaur, S.M. Lawrie, Towards a neuroanatomy of autism: a systematic review and meta-analysis of structural magnetic resonance imaging studies, European Psychiatry 23 (4) (2008) 289–299.
[7] L. Bonilha, F. Cendes, C. Rorden, M. Eckert, P. Dalgalarrondo, L.M. Li, C.E. Steiner, Gray and white matter imbalance—typical structural abnormality underlying classic autism?, European Psychiatry 30 (6) (2008) 396–401.
[8] G.M. McAlonan, J. Suckling, N. Wong, V. Cheung, N. Lienenkaemper, C. Cheung, S.E. Chua, Distinct patterns of grey matter abnormality in high-functioning autism and Asperger's syndrome, Journal of Child Psychology and Psychiatry 49 (12) (2008) 1287–1295.
[9] D.C. Rojas, E. Peterson, E. Winterrowd, M.L. Reite, S.J. Rogers, J.R. Tregellas, Regional gray matter volumetric changes in autism associated with social and repetitive behavior symptoms, BMC Psychiatry 6 (56) (2006).
[10] A.Y. Hardan, S. Muddasani, M. Vemulapalli, M.S. Keshavan, N.J. Minshew, An MRI study of increased cortical thickness in autism, American Journal of Psychiatry 163 (7) (2006) 1290–1292.
[11] J.E. Lainhart, Advances in autism neuroimaging research for the clinician and geneticist, American Journal of Medical Genetics Part C: Seminars in Medical Genetics 142C (1) (2006) 33–39.
[12] A.R. Brito, M.M. Vasconcelos, R.C. Domingues, L.C.J. Hygino da Cruz, L.d.S. Rodrigues, E.L. Gasparetto, C.A.B.P. Calçada, Diffusion tensor imaging findings in school-aged autistic children, Journal of Neuroimaging 19 (4) (2009) 337–343.
[13] T.W. Frazier, A.Y. Hardan, A meta-analysis of the corpus callosum in autism, Biological Psychiatry 66 (10) (2009) 935–941.
[14] M.A. Just, V.L. Cherkassky, T.A. Keller, N.J. Minshew, Cortical activation and synchronization during sentence comprehension in high-functioning autism: evidence of underconnectivity, Brain 127 (8) (2004) 1811–1821.
[15] M.A. Just, V.L. Cherkassky, T.A. Keller, R.K. Kana, N.J. Minshew, Functional and anatomical cortical underconnectivity in autism: evidence from an fMRI study of an executive function task and corpus callosum morphometry, Cerebral Cortex 17 (4) (2007) 951–961.
[16] R.K. Kana, T.A. Keller, V.L. Cherkassky, N.J. Minshew, M.A. Just, Sentence comprehension in autism: thinking in pictures with decreased functional connectivity, Brain 129 (9) (2006) 2484–2493.
[17] H. Koshino, R.K. Kana, T.A. Keller, V.L. Cherkassky, N.J. Minshew, M.A. Just, fMRI investigation of working memory for faces in autism: visual coding and underconnectivity with frontal areas, Cerebral Cortex 18 (2) (2008) 289–300.
[18] N.M. Kleinhans, T. Richards, L. Sterling, K.C. Stegbauer, R. Mahurin, L.C. Johnson, J. Greenson, G. Dawson, E. Aylward, Abnormal functional connectivity in autism spectrum disorders during face processing, Brain 131 (4) (2008) 1000–1012.
[19] B. Wicker, P. Fonlupt, B. Hubert, C. Tardif, B. Gepner, C. Deruelle, Abnormal cerebral effective connectivity during explicit emotional processing in adults with autism spectrum disorder, Social Cognitive & Affective Neuroscience 3 (2) (2008) 135–143.
[20] A. Mizuno, M.E. Villalobos, M.M. Davies, B.C. Dahl, R.-A. Müller, Partially enhanced thalamocortical functional connectivity in autism, Brain Research 1104 (1) (2006) 160–174.
[21] S.K. Noonan, F. Haist, R.-A. Müller, Aberrant functional connectivity in autism: evidence from low-frequency bold signal fluctuations, Brain Research 1262 (2009) 48–63.
[22] D.P. Kennedy, E. Courchesne, The intrinsic functional organization of the brain is altered in autism, NeuroImage 39 (4) (2008) 1877–1885.
[23] C.S. Monk, S.J. Peltier, J.L. Wiggins, S.-J. Weng, M. Carrasco, S. Risi, C. Lord, Abnormalities of intrinsic functional connectivity in autism spectrum disorders, NeuroImage 47 (2) (2009) 764–772.
[24] S.-J. Weng, J.L. Wiggins, S.J. Peltier, M. Carrasco, S. Risi, C. Lord, C.S. Monk, Alterations of resting state functional connectivity in the default network in adolescents with autism spectrum disorders, Brain Research 1313 (2010) 202–214.
[25] M. Murias, S.J. Webb, J. Greenson, G. Dawson, Resting state cortical connectivity reflected in EEG coherence in individuals with autism, Biological Psychiatry 62 (3) (2007) 270–273.
[26] R. Coben, A.R. Clarke, W. Hudspeth, R.J. Barry, EEG power and coherence in autistic spectrum disorder, Clinical Neurophysiology 119 (5) (2008) 1002–1009.

[27] J.D. Lewine, R. Andrews, M. Chez, A.-A. Patil, O. Devinsky, M. Smith, A. Kanner, J.T. Davis, M. Funke, G. Jones, B. Chong, S. Provencal, M. Weisend, R.R. Lee, W.W. Orrison Jr., Magnetoencephalographic patterns of epileptiform activity in children with regressive autism spectrum disorders, Pediatrics 104 (3) (1999) 405–418.
[28] J. Muñoz-Yunta, T. Ortiz, M. Palau-Baduell, L. Martín-Muñoz, B. Salvadó-Salvadó, A. Valls-Santasusana, J. Perich-Alsina, I. Cristóbal, A. Fernández, F. Maestú, C. Dürsteler, Magnetoencephalographic pattern of epileptiform activity in children with early-onset autism spectrum disorders, Clinical Neurophysiology 119 (3) (2008) 626–634.
[29] A.P. Georgopoulos, E. Karageorgiou, A.C. Leuthold, S.M. Lewis, J.K. Lynch, A.A. Alonso, Z. Aslam, A.F. Carpenter, A. Georgopoulos, L.S. Hemmy, I.G. Koutlas, F.J.P. Langheim, J.R. McCarten, S.E. McPherson, J.V. Pardo, P.J. Pardo, G.J. Parry, S.J. Rottunda, B.M. Sega, S.R. Sponheim, J.J. Stanwyck, M. Stephane, J.J. Westermeyer, Synchronous neural interactions assessed by magnetoencephalography: a functional biomarker for brain disorders, Journal of Neural Engineering 4 (4) (2007) 349–355.
[30] M. Rubinov, O. Sporns, Complex network measures of brain connectivity: uses and interpretations, NeuroImage 52 (3) (2010) 1059–1069.
[31] A.A. Ioannides, Dynamic functional connectivity, Current Opinion in Neurobiology 17 (2) (2007) 161–170.
[32] P.L. Nunez, R. Srinivasan, A.F. Westdorp, R.S. Wijesinghe, D.M. Tucker, R.B. Silberstein, P.J. Cadusch, EEG coherency I: statistics, reference electrode, volume conduction, Laplacians, cortical imaging, and interpretation at multiple scales, Electroencephalography and Clinical Neurophysiology 103 (5) (1997) 499–515.
[33] E. Pereda, R. Quian Quiroga, J. Bhattacharya, Nonlinear multivariate analysis of neurophysiological signals, Progress in Neurobiology 77 (1–2) (2005) 1–37.
[34] O. David, D. Cosmelli, K.J. Friston, Evaluation of different measures of functional connectivity using a neural mass model, NeuroImage 21 (2) (2004) 659–673.
[35] J. Arnhold, P. Grassberger, K. Lehnertz, C.E. Elger, A robust method for detecting interdependences: application to intracranially recorded EEG, Physica D 134 (4) (1999) 419–430.
[36] R. Quian Quiroga, A. Kraskov, T. Kreuz, P. Grassberger, Performance of different synchronization measures in real data: a case study on electroencephalographic signals, Physical Review E 65 (4) (2002) 041903.
[37] F. Takens, Detecting strange attractors in turbulence, in: Dynamical Systems and Turbulence, vol. 898, 1981, pp. 366–381 (Lecture Notes in Mathematics).
[38] J. Theiler, Spurious dimension from correlation algorithms applied to limited time-series data, Physical Review A 34 (3) (1986) 2427–2432.
[39] R. Hegger, H. Kantz, T. Schreiber, Practical implementation of nonlinear time series methods: the TISEAN package, Chaos 9 (2) (1999) 413–435.
[40] A.M. Fraser, H.L. Swinney, Independent coordinates for strange attractors from mutual information, Physical Review A 33 (2) (1986) 1134–1140.
[41] M.B. Kennel, R. Brown, H.D.I. Abarbanel, Determining embedding dimension for phase-space reconstruction using a geometrical construction, Physical Review A 45 (6) (1992) 3403–3411.
[42] P. Grassberger, Finite sample corrections to entropy and dimension estimates, Physics Letters A 128 (6–7) (1988) 369–373.
[43] S.P. Strong, R. Koberle, R.R. de Ruyter van Steveninck, W. Bialek, Entropy and information in neural spike trains, Physical Review Letters 80 (1) (1998) 197–200.
[44] L. Paninski, Estimation of entropy and mutual information, Neural Computation 15 (6) (2003) 1191–1253.
[45] N. Slonim, G.S. Atwal, G. Tkacik, W. Bialek, Estimating mutual information and multi-information in large networks, Arxiv preprint cs/0502017 〈http://www.genomics.princeton.edu/biophysics-theory/DirectMI/web-content/index.html〉, 2005.
[46] K. Hlaváčková–Schindler, M. Paluš, M. Vejmelka, J. Bhattacharya, Causality detection based on information-theoretic approaches in time series analysis, Physics Reports 441 (1) (2007) 1–46.
[47] L.A. Baccalá, K. Sameshima, Partial directed coherence: a new concept in neural structure determination, Biological Cybernetics 84 (6) (2001) 463–474.
[48] L.A. Baccalá, K. Sameshima, D.Y. Takahashi, First public release of the PDC package, URL 〈http://www.lcs.poli.usp.br/∼ baccala/pdc/〉, 2007.
[49] E. Bullmore, O. Sporns, Complex brain networks: graph theoretical analysis of structural and functional systems, Nature Reviews Neuroscience 10 (3) (2009) 186–198.
[50] C.J. Stam, J.C. Reijneveld, Graph theoretical analysis of complex networks in the brain, Nonlinear Biomedical Physics 1 (3) (2007).
[51] V. Tsiaras, Algorithms for the analysis and visualization of biomedical networks, Ph.D. Thesis, Computer Science Department, University of Crete, 2009.
[52] D.J. Watts, S.H. Strogatz, Collective dynamics of 'small-world' networks, Nature 393 (6684) (1998) 440–442.
[53] B. Zhang, S. Horvath, A general framework for weighted gene co-expression network analysis, Statistical Applications in Genetics and Molecular Biology 4 (1) (2005).
[54] M.E.J. Newman, Assortative mixing in networks, Physical Review Letters 89 (20) (2002) 208701.
[55] C.C. Leung, H.F. Chau, Weighted assortative and disassortative networks model, Physica A 378 (2) (2007) 591–602.
[56] V. Latora, M. Marchiori, Efficient behavior of small-world networks, Physical Review Letters 87 (19) (2001) 198701.
[57] V. Latora, M. Marchiori, Economic small-world behavior in weighted networks, The European Physical Journal B 32 (2) (2003) 249–263.
[58] G. Fagiolo, Clustering in complex directed networks, Physical Review E 76 (2) (2007) 026107.
[59] M. Piraveenan, M. Prokopenko, A.Y. Zomaya, Assortative mixing in directed networks, Tech. Rep. 637, The University of Sydney 〈http://www.it.usyd.edu.au/research/tr/tr637.pdf〉, 2009.
[60] C.-h. Park, S.Y. Kim, Y.-H. Kim, K. Kim, Comparison of the small-world topology between anatomical and functional connectivity in the human brain, Physica A 387 (23) (2008) 5958–5962.
[61] B. Schelter, M. Winterhalder, M. Eichler, M. Peifer, B. Hellwig, B. Guschlbauer, C.H. Lücking, R. Dahlhaus, J. Timmer, Testing for directed influences among neural signals using partial directed coherence, Journal of Neuroscience Methods 152 (1–2) (2006) 210–219.
[62] D.Y. Takahashi, L.A. Baccalá, K. Sameshima, Connectivity inference between neural structures via partial directed coherence, Journal of Applied Statistics 34 (10) (2007) 1259–1273.
[63] R.G. Andrzejak, A. Kraskov, H. Stögbauer, F. Mormann, T. Kreuz, Bivariate surrogate techniques: necessity, strengths, and caveats, Physical Review E 68 (6) (2003) 066202.
[64] M.A. Coskun, L. Varghese, S. Reddoch, E.M. Castillo, D.A. Pearson, K.A. Loveland, A.C. Papanicolaou, B.R. Sheth, How somatic cortical maps differ in autistic and typical brains, NeuroReport 20 (2) (2009) 175–179.
[65] C. Lord, M. Rutter, P.C. DiLavore, S. Risi, Autism Diagnostic Observation Schedule (ADOS) Manual, Western Psychological Services, Los Angeles, 1999.
[66] M. Rutter, A. Le Couteur, C. Lord, Autism Diagnostic Interview—Revised Manual, The Psychological Corporation, Western Psychological Services, Los Angeles, 2003.
[67] D. Wechsler, Wechsler Abbreviated Scale of Intelligence Manual, San Antonio, Texas, 1999.
[68] T.W. Wilson, D.C. Rojas, M.L. Reite, P.D. Teale, S.J. Rogers, Children and adolescents with autism exhibit reduced MEG steady-state gamma responses, Biological Psychiatry 62 (3) (2007) 192–197.
[69] N.M. Gage, B. Siegel, M. Callen, T.P.L. Roberts, Cortical sound processing in children with autism disorder: an MEG investigation, NeuroReport 14 (16) (2003) 2047–2051.
[70] T.P. Roberts, S.Y. Khan, M. Rey, J.F. Monroe, K. Cannon, L. Blaskey, S. Woldoff, S. Qasmieh, M. Gandal, G.L. Schmidt, D.M. Zarnow, S.E. Levy, J.C. Edgar, MEG detection of delayed auditory evoked responses in autism spectrum disorders: towards an imaging biomarker for autism, Autism Research 3 (1) (2010) 8–18.
[71] L. Pollonini, U. Patidar, N. Situ, R. Rezaie, A.C. Papanicolaou, G. Zouridakis, Functional connectivity networks in the autistic and healthy brain assessed using Granger causality, in: Annual International Conference of the IEEE EMBC (2010), 2010, pp. 1730–1733.